

Article

Assessment of Sorption of Anthocyanins from Red Cabbage onto Bentonites from Patagonia (Argentina)

Vanina Rodríguez-Ameijide¹, Andrea Maggio^{1,2}, Manuel Pozo^{3,*} , M. Belén Gómez¹, Pablo M. Naranjo⁴ and M. Eugenia Roca-Jalil^{1,2,*}

¹ Department of Chemistry, Faculty of Engineering, National University of Comahue, Neuquén 8300, Argentina; vanina.rodriguez@fain.uncoma.edu.ar (V.R.-A.); andreamaggio8@gmail.com (A.M.)

² Institute of Research and Development in Process Engineering, Biotechnology, and Alternative Energies (PROBIEN, CONICET-UNCo), Neuquén 8300, Argentina

³ Department of Geology and Geochemistry, Faculty of Sciences, Autonomous University of Madrid, Campus de Cantoblanco, 28049 Madrid, Spain

⁴ Institute of Research for the Chemical Industry (INIQUI), Av. Bolivia 5150, Salta A4408FVY, Argentina; pmnaranjo@gmail.com

* Correspondence: manuel.pozo@uam.es (M.P.); merocajalil@gmail.com (M.E.R.-J.); Tel.: +34-914974808 (M.P.); Tel./Fax: +54-2994490300 (M.E.R.-J.)



Citation: Rodríguez-Ameijide, V.; Maggio, A.; Pozo, M.; Gómez, M.B.; Naranjo, P.M.; Roca-Jalil, M.E. Assessment of Sorption of Anthocyanins from Red Cabbage onto Bentonites from Patagonia (Argentina). *Minerals* **2024**, *14*, 133. <https://doi.org/10.3390/min14020133>

Academic Editor: Felix Brandt

Received: 30 December 2023

Revised: 19 January 2024

Accepted: 20 January 2024

Published: 25 January 2024

Correction Statement: This article has been republished with a minor change. The change does not affect the scientific content of the article and further details are available within the backmatter of the website version of this article.



Copyright: © 2024 by the authors. Licensee MDPI, Basel, Switzerland. This article is an open access article distributed under the terms and conditions of the Creative Commons Attribution (CC BY) license (<https://creativecommons.org/licenses/by/4.0/>).

Abstract: In the northern Patagonian region of Argentina, some of the largest bentonite deposits exist. Four bentonite samples (B1, B2, B3, and B4) from two deposits were thoroughly characterised and evaluated as potential adsorbents of anthocyanins extracted from red cabbage. Anthocyanins (ACys) are natural colourants obtained from fruits and plants and have shown excellent antioxidant properties that have promising applications in health. The adsorption of ACys onto bentonites enhances their stability relative to that observed in aqueous solutions. Material characterisation showed that three of the samples are soFidium bentonites (Na-bentonites: B2, B3, and B4), while the fourth exhibits a large quantity of magnesium and calcium in its interlayer, classifying it as a Mg-Ca-Na-bentonite (B1). Na-bentonites demonstrated higher ACy adsorption capacities, occurring through cation exchange, while Mg-Ca-Na-bentonite adsorption occurs by another type of interaction and a cooperative adsorption mechanism, resulting in the lowest ACy adsorption. The highest adsorption capacity was noted for B3, characterised by the highest smectite content, cation exchange capacity, and proportion of monovalent cations in its interlayer. Under the conditions studied, sodium smectites proved to be capable of retaining red cabbage ACys, thereby introducing a novel avenue for potential applications of regional materials with potential implications for health-related uses.

Keywords: bentonites; anthocyanins; adsorption from water

1. Introduction

Anthocyanins (ACys) are pigments responsible for the blue, purple, and red hues in various plants, fruits, and vegetables. These organic compounds, serving as natural dyes, have garnered attention for their easy extraction, non-toxicity, and water solubility, positioning them as potential substitutes for synthetic dyes in the food industry [1,2]. Beyond their coloration properties, ACys exhibit biological activities associated with health benefits, including antioxidant, antidiabetic, and cardioprotective properties [2–6]. Chemically classified as flavonoids, ACy structures incorporate cyanidin, delphinidin, and pelargonidin nuclei or their methylated derivatives. Typically, ACys are glycosides of anthocyanidins, with only a select few found in fruits and vegetables [2,6,7].

The ACys from red cabbage have acquired special attention owing to potential applications linked to physiological functions. Red cabbage exhibits a higher ACy content compared to other vegetables, influenced by variables such as variety, crop type, and

maturation time [2,6,8]. In aqueous solutions, ACys are compounds extremely sensitive to variations in pH, manifesting at least five distinct colours and serving as natural pH indicators [1,9–13]. However, the pH indicator properties along with the health benefits of ACys are limited based on their stability in water, which depends on factors like pH, temperature, and light intensity. Consequently, there are studies focused on identifying solid supports for ACys that could preserve their properties and enhance stability [1,9–13].

Clay minerals have emerged as promising candidates among various solids studied, demonstrating efficacy in improving ACy stability and fostering the exploration of novel applications [11–13].

In recent years, Argentina has been the second largest producer of bentonites in South America, exporting this product to more than a dozen countries [14]. The largest bentonite deposit is located in the Patagonia region where the Rio Negro province has the highest extraction and industrial activities. In this region, sodium or mixtures of sodium and calcium bentonites (Na/Ca) are commonly mined. They are considered to be materials of a high purity due to their high smectite content [15,16]. The regional bentonites are used mostly for typical industrial applications, such as additives to moulding sands; drilling fluid thickeners in the oil industry; clarifiers for wines, juices and cooking oils; and additives in pet food. Due to their low cost, abundance, and environmental compatibility, bentonites from North Patagonia have been studied and shown to be good adsorbents of different organic and inorganic species in water [17–22]. Despite the wide use of different clay minerals as excipients and active principles in the pharmaceutical and cosmetic industry, in addition to their applications in drug-carrying and -release methods and pelotherapy [23–25], there are only a few studies related to the potential use of regional bentonites [26,27].

In this study, four bentonites sourced from distinct deposits in the Patagonian region of Argentina were characterised and assessed as potential solid supports for ACy extracted from red cabbage. The adsorption studies aimed to identify the most effective adsorbent material to enhance the stability of the retained ACys and assess potential novel applications for the resulting ACy–clay complex. The latter presents an intriguing prospect for regional materials, offering new applications that have not been explored thus far and could have a significant impact on the regional industry.

2. Materials and Methods

2.1. Bentonite Samples

Four cretaceous bentonites from the Patagonian region were analysed and designated as B1, B2, B3, and B4. The first was collected from the Cerro Valcheta site in the Río Negro province belonging to the Neuquén Group (NG) [28,29]. The other three were collected from different locations in the Allen Formation (AF). Specifically, B2 was obtained from a location near the town of Catriel, and B3 and B4 were obtained from deposits in Lake Pellegrini. The locations are shown in Figure 1.

2.2. Anthocyanin Properties and Extraction

Chemically, ACys belong to the flavonoid family sharing the same nucleus of phenolic rings but differing in their substituent groups. Usually, an extract taken from natural sources will contain a mix of ACys, which in the case of red cabbage included more than 30 different components. All the ACys present in red cabbage are derived from the main component, namely, cyanidin-3-diglucoside-5-glucoside (Figure 2), where the acyl groups act as protectors of the flavylium cation, thus preventing its degradation and generating unusual stability under different media pH [2,3]. The chromophore responsible for the anthocyanin dye is the flavylium cation, which changes the colour of the solution depending on the substituents present in their structure and the Acy source [3]. In the case of red cabbage, four species are possible depending on the media pH. At pH values lower than 3, the solution becomes red due to the presence of flavylium cation and its hydration. At pH values between 3 and 9, it generates a carbinol pseudobase and quinoidal

bases, and the colour of the solution changes from violet to blue. The last species has a chalcone pseudobase and its presence turns the colour of the solution to yellow. The latter is associated with the rupture of the anthocyanin chromophore and its degradation, which is generated by pH values higher than 9 or at high temperatures [2,3,6,8].

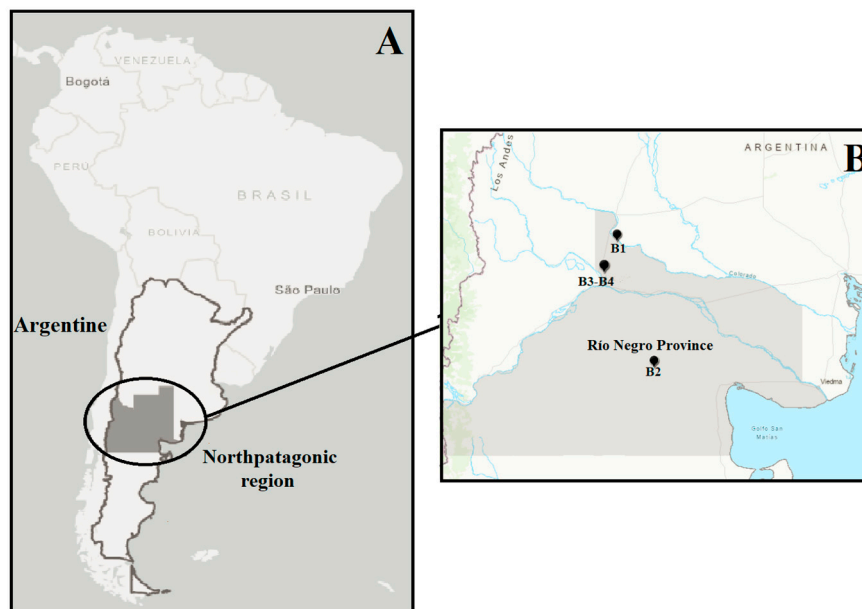


Figure 1. (A) North Patagonia region in Argentina. (B) Sampling location in Rio Negro Province where B1 (Cerro Valcheta), B2 (Catriel), and B3 and B4 (Pellegrini Lake) were obtained.

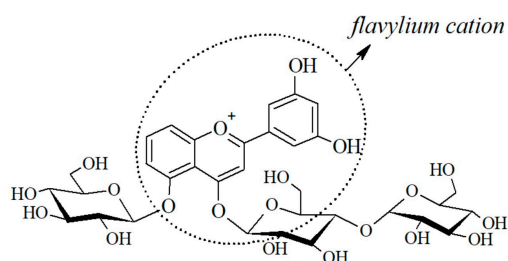


Figure 2. Chemical structure of cyanidin-3-diglucoside-5-glucoside.

A red cabbage extract was prepared using simple extraction with water. The system was prepared with 500 g of washed, cleaned, and crushed red cabbage with distilled water at a ratio of 0.8:1 g mL⁻¹. The mixture was covered and heated by boiling for 45 min. After filtering, the supernatant was adjusted to pH 3 with hydrochloric acid (0.1 mol L⁻¹) and was kept covered from light and frozen until use. The ACy concentration was measured using a T60 UV-VIS spectrophotometer and following the methodology proposed by Giusti and Wrolstad (2001) [30].

2.3. Characterisation of Bentonite Samples

2.3.1. Mineralogical, Chemical and Structural Characterisation

Mineralogical analysis of the four samples was carried out using X-ray diffraction (XRD) in a Bruker D8 with Lynxeye XE-T detector equipment, (Billerica, MA, USA) with CuK α radiation (40 kV, 20 mA) and a scanning speed of 1° 2 θ /min. The powdered whole-rock samples were used to determine bulk mineralogy. After clay fraction separation (<2 μ m), sample mounts were prepared from suspensions oriented on glass slides. The identification of clay minerals was carried out on the air-dried (AD) samples with ethylene glycol solvation (EG) and heated at 550 °C. The mineral intensity factor (MIF) method was applied to XRD reflection intensity ratios normalised to 100% with calibration constants

for the quantitative estimation of mineral content [31]. To establish the relative ordering ‘crystallinity’ of smectite, the full width at half maximum (FWHM) parameter was measured using the (001) reflection on the ethylene glycol oriented mount [32]. The crystallite size was calculated using the Scherrer equation.

In addition to the XRD technique, the mineralogical analysis was complemented with infrared spectroscopy (FTIR), thermal analysis (DTA-TGA), and nuclear magnetic resonance analysis (NMR). Thermal analysis (DSC/DTA/TGA Q600 of TA Instruments, Newcastle, DE, USA) of the four samples was performed using 10 mg powdered clay sample in a Pt sample holder at an average heating rate of 10 °C/min with an alumina reference. The infrared spectroscopy (FTIR) (Bruker IFS 66v standard, Karlsruhe, Germany) spectra of the same four representative samples were recorded with a spectral resolution of 2 cm⁻¹ in transmission mode in the 400–4000 cm⁻¹ region. The samples were examined in KBr pellets (3 mg/300 mg KBr). Nuclear magnetic resonance analysis ²⁷Al (NMR) (Bruker Av 400 WB, Fällanden, Switzerland) of the clay fraction was also carried out. The ²⁷Al MAS NMR spectra were recorded with pi/12 excitation pulses to obtain a response as uniform as possible for both octahedral and tetrahedral aluminium [33].

Chemical analyses of the four whole-rock bentonites were carried out using sample fusion and inductively coupled plasma atomic emission spectroscopy (ICP-AES and MS) for major and trace elements at the ACTLABS laboratory (Ancaster, ON, Canada). The detection limits for analyses were between 0.01 and 0.001 wt.% for major elements.

2.3.2. Physical and Physicochemical Properties

The physical and physicochemical properties of the bentonite samples, such as cation exchange capacity, swelling, water content, granulometry, and colour, were studied. The cation exchange capacity (CEC) was measured using the copper triethylenetetramine [Cu(trien)]²⁺ method [34] where 0.025 g of previously dried mineral was suspended in 5 mL distilled water, and a solution 0.01 mol L⁻¹ [Cu(trien)]²⁺ was used for the exchange at pH 7. The swelling capacity was determined according to the ASTM 5890 rule. The water content was gravimetrically measured, and 0.25 g mineral was dried at 60 °C under a controlled air atmosphere until a constant weight was achieved. The sample colour was determined using a Minolta CR 400 photocolourimeter. The grain size distribution of the samples was determined using a laser diffraction analyser (Malvern Mastersizer3000, Almelo, The Netherlands) in the 0.01–1000 µm range. The statistical parameters considered were the mode, median (Dv50), volume mean diameter D [3,4], and Dv90 percentiles.

2.4. Anthocyanin Adsorption Assays

The adsorption experiments were conducted by mixing 0.02 g adsorbent with 8 mL ACy solution in 10 mL tubes and stirring at 20 °C until the equilibrium time was reached. The adsorbent–solution relationship was selected based on previous studies [20]. After adsorption, the supernatants were separated using a Sorvall RC 5C centrifuge at 8000 rpm for 20 min. The ACy equilibrium concentrations were measured using a T60 UV-VIS spectrophotometer following the methodology proposed by Giusti and Wrolstad (2001) [30]. All samples were measured in duplicate, and the average value is presented in the results. The quantity of adsorbed ACys was calculated according to Equation (1):

$$q = \frac{V \times (C_i - C_e)}{w} \quad (1)$$

where V is the ACy solution volume (L); C_i and C_e are initial and equilibrium ACy concentrations (mmol L⁻¹), respectively; and w is the mass of adsorbent (g).

Different authors have reported the low stability of ACy solutions at pH values higher than 6; therefore, this pH range was not studied [1,35]. The first test was carried out on all samples in contact with 0.75 mM ACy solution at pH 3 and stirring for 24 h. From these results, the sample that showed the greatest adsorption was selected to evaluate the effect of pH on adsorption using a 0.5 mM ACy solution adjusted to pH values between

3 and 6 with either HCl or NaOH and stirring at 20 °C for 24 h. Following this, kinetic experiments were conducted with an ACy solution at 0.38 mM, and the contact times varied between 0.5 and 24 h. Taking into account all the previous results, the adsorption isotherms were carried out using ACy solutions from 0.12 to 1.3 mM at pH 3 and a 5 h contact time. The experimental results for the adsorption kinetics were fitted to both the pseudo-first-order (PFO) and pseudo-second-order models (PSO), and the adsorption isotherm data were fitted to Langmuir, Freundlich, and Sips isotherm models to evaluate the adsorption mechanism of Acy on the bentonites [36–38].

3. Results and Discussion

3.1. Material Characterisation

3.1.1. Mineralogical, Chemical, and Structural Characterisation

Mineralogical results from the four samples analysed are shown in Figure 3 and Table 1. Phyllosilicates were dominant (88%–95%) with a mean value of 93%. The minerals quartz (tr-3%), feldspar (plagioclase and/or potassium feldspar) (tr-2%), and gypsum (0%–4%), occurred as minor phases. In sample B1, trydimite (10%) was also identified.

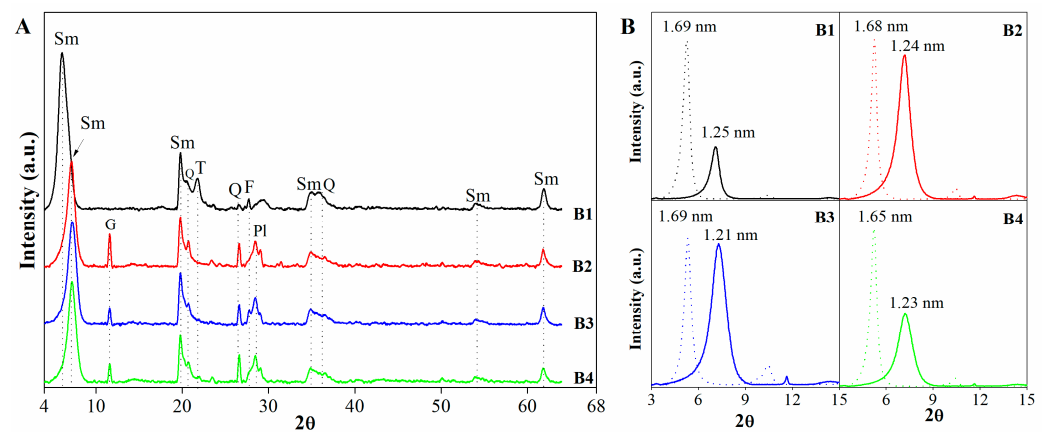


Figure 3. (A). Representative powder X-ray pattern of the bentonites. Sm: smectite; Q: quartz; Pl: plagioclase; F: potassic feldspars; G: gypsum. (B). Diffractograms of <2 μm grain-size fraction for bentonites, solid lines represent air-dried (AD) samples, and dotted lines represent samples after ethylene glycol solvation (EG).

Table 1. Bentonite mineralogy determined by XRD (% w/w), characteristic basal spaces (d_{001} and d_{060}), FWHM values ($\circ 2\theta$), crystallite sizes (Cr) (nm), and weight loss from TGA are also shown. (Tr. < 0.1%).

	Mineralogy (% w/w)					Basal d-Spacing (nm)		Smectite Crystallinity		Weight Loss (%)		
	Sm	Gy	Qz	Try	F	d_{001}	d_{060}	FWHM	Cr	20–200 °C	200–1000 °C	Total
B1	88	0	Tr.	10	2	1.456	0.1498	0.47	18	9.21	4.20	13.42
B2	94	4	2	0	Tr.	1.247	0.1499	0.40	20	5.01	4.50	9.51
B3	95	2	2	0	1	1.224	0.1498	0.49	17	1.97	6.31	8.28
B4	95	2	3	0	Tr.	1.224	0.1498	0.44	18	4.19	9.00	13.20

Sm: Smectite, Gy: Gypsum, Qz: Quartz; Try: Trydimite, F: Feldspars.

The clay fraction (<2 μm) was mainly composed of smectite (>88%), which was the only clay mineral present. The oriented clay samples B2, B3, and B4 showed the presence of dioctahedral Al-smectite ($d_{060} = 0.1498\text{--}0.1499$ nm) with Na as the main interlayer cation ($d_{001} = 1.224\text{--}1.247$ nm). In sample B1, the dioctahedral Al-smectite ($d_{060} = 0.1498$ nm) had mostly divalent cations as interlayer cations ($d_{001} = 1.456$ nm). The characteristic basal d-spacings of ethylene glycol solvated samples were 1.663–1.691 nm (001), 0.841–0.848 nm

(002), 0.559–0.563 nm (003), 0.421–0.424 nm (004), and 0.335–0.338 nm (005). The FWHM parameter of the ethylene glycolated smectites was variable in the bentonite samples, ranging from 0.40 to 0.49 and corresponding to crystallite sizes between 18 and 21 nm. The Greene–Kelly test corroborates the presence of an octahedral high-charge smectite of the montmorillonite type [39].

The chemical composition of the bentonites is shown in Table 2. The samples showed major element contents consistent with the identified mineralogy. Significant differences were observed between the analysis of B1 and the other samples. The sample formed by smectite with Na in the interlayer (B2, B3, and B4) presented a lower SiO₂ (54.14%–55.19%) and MgO (2.59%–2.78%) content but a higher Al₂O₃ (16.78%–17.62%), Fe₂O₃ (4.18%–4.38%), CaO (1.11%–2.21%), Na₂O (2.21%–2.68%), K₂O (0.28%–0.36%), and TiO₂ (0.20%–0.52%) content. The SiO₂/Al₂O₃ and Na₂O/MgO molar ratios were different, with B1 reaching 6.81 and 0.19, respectively. In the remaining samples, a lower SiO₂/Al₂O₃ (5.30–5.48) but higher Na₂O/MgO (0.51–0.67) molar ratio were observed. In addition to the observed difference in the interlayer cations and the absence of gypsum in B1, it is obvious that there is a genetic factor that would justify the compositional differences. The average structural formulae of analysed bentonites are presented in Table 2, corroborating that smectite is montmorillonite in all samples.

Table 2. Chemical composition (% w/w of each major element oxide) and structural formulae of samples.

Sample	%	SiO ₂	Al ₂ O ₃	Fe ₂ O ₃	MnO	MgO	CaO	Na ₂ O	K ₂ O	TiO ₂	P ₂ O ₅	LOI
B1		58.49	14.58	1.09	0.031	4.19	1.09	1.28	0.26	0.158	<0.01	17.41
B2		54.14	16.78	4.38	0.017	2.78	1.79	2.21	0.36	0.526	0.19	15.42
B3		55.29	17.62	4.18	0.043	2.67	1.11	2.68	0.28	0.198	0.06	15.15
B4		54.56	16.99	4.26	0.044	2.59	2.21	2.67	0.30	0.257	0.08	14.76

B1 (Si₈)_{IV}(Al_{2.80}Fe_{0.14}Mg_{1.10}Mn_{0.005}Ti_{0.02})_{VI}O₂₀(OH)₄M^{+0.96}. **B2** (Si_{7.92}Al_{0.08})_{IV}(Al_{2.81}Fe_{0.48}Mg_{0.61}Mn_{0.002}Ti_{0.06})_{VI}O₂₀(OH)₄M^{+0.72}. **B3** (Si_{7.93}Al_{0.07})_{IV}(Al_{2.88}Fe_{0.46}Mg_{0.51}Mn_{0.005}Ti_{0.02})_{VI}O₂₀(OH)₄M^{+0.79}. **B4** (Si_{7.87}Al_{0.13})_{IV}(Al_{2.76}Fe_{0.46}Mg_{0.56}Mn_{0.005}Ti_{0.03})_{VI}O₂₀(OH)₄M^{+1.02}.

Figure 4 shows the FTIR spectra for the samples. All spectra showed montmorillonite characteristic signals, which are summarised in Table 3 and compared with the Wyoming bentonite samples as a reference [40].

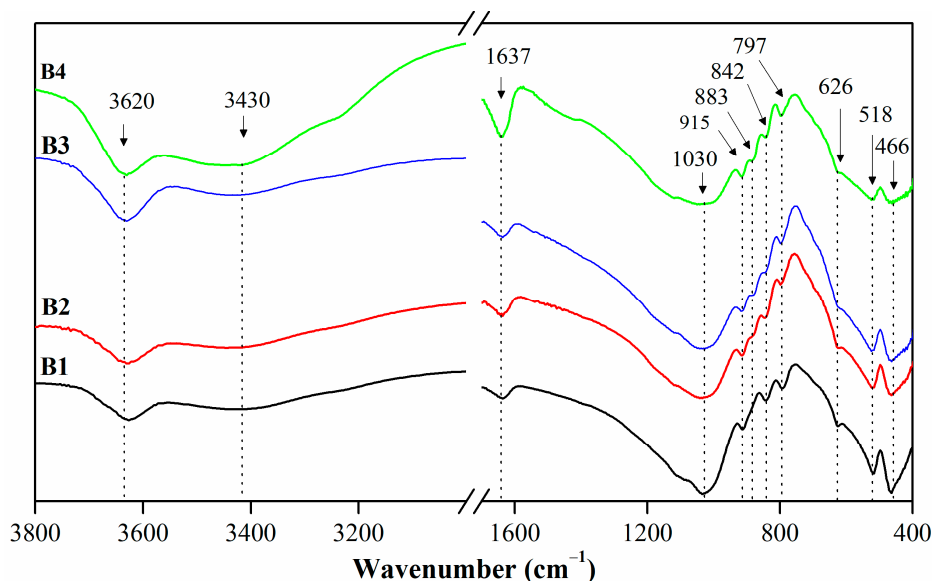


Figure 4. FTIR spectra for the four bentonites.

Table 3. FTIR spectral data for the samples using Wyoming bentonite as a reference [40].

Assignment	Sample (cm ⁻¹)				
	B1	B2	B3	B4	Wy
ν Al(or Mg)-OH	3623	3620	3620	3620	3631
ν H-O-H	3430	3430	3430	3430	3442
δ H-O-H	1637	1637	1637	1637	1640
ν Si-O	1030	1030	1030	1030	1045
δ Al-Mg-OH	915	915	915	915	919
δ Fe-Al-OH	---	883	883	883	---
δ Al-Al-OH	845	845	849	845	843
ν Si-O	791	797	797	797	798
δ Si-O and Al-O	626	626	626	626	---
δ Al-O-Si	525	525	525	525	---
δ Si-O-Si	463	463	463	463	463

The bands observed with the highest wavenumber were associated with the O-H stretching and bending vibrations of the water molecules adsorbed on the inner and outer montmorillonite surfaces. Additionally, all spectra showed bands assigned to stretching Si-O bonds and Si-O-Si stretching vibration for dioctahedral smectites and the bands associated with the presence of aluminium in the tetrahedral sheets (δ Al-O-Si and δ Al-O-Si). The OH bending of Al-(or Mg)-OH and Al-OH-Al were identified and associated with the presence of octahedral cations. In the case of B1, both the slight displacement of the 3620 cm⁻¹ band towards a lower wavenumber and the absence of the 885 cm⁻¹ band (stretching Fe-Al-OH) are characteristic of Mg-Ca montmorillonite, in agreement with the DRX and the chemical results [40–42].

The TGA curves of the samples were typical for Al-smectite [43], showing very similar thermal behaviour (Figure 5). Two characteristic weight loss ranges were obtained for all the samples and are summarised in Table 1. The first one appeared between 20 and 200 °C and is related to the loss of physisorbed water. All the samples showed two peaks below 200 °C. In the cases of B2, B3, and B4, the peak observed at 53 °C is associated with the sample humidity, and the peak at 105 °C suggests the prevalence of monovalent interlayer cations. Sample B1 showed the highest weight loss in this range (9.21%), and the temperature for the second peak was 130 °C, providing evidence that this sample has a greater amount of ab-adsorbed water. This is due to the presence of divalent cations in the clay interlayer, which have a greater polarizing power than monovalent cations and therefore retain water more strongly [40,44,45]. The second weight loss range was between 200 and 1000 °C and has been assigned to the incipient dehydroxylation of calcium and sodium montmorillonites, which can appear at different temperatures according to the interlayer cation. In this range, the TGAs of B1 and B2 showed one peak at 642 and 660 °C, respectively, whereas B3 and B4 exhibited two peaks around 570 and 650 °C, all of which are associated with the removal of structural OH in the clay mineral structure. Usually, this behaviour is also associated with the presence of iron in the samples and is commonly related to the genetic type of their deposit [40,44].

The NMR spectra of the solids provide unique information about the structure and dynamics of the materials under study. The ²⁷Al MAS spectra of bentonites exhibit a large peak at around 0.86 ppm for B1 but ranged between 2.89 and 3.92 ppm for B2 and B4, indicating that much of the aluminium is in the octahedral Al environments [46], corroborating the montmorillonite composition of the smectite in both the Mg-Ca and Na bentonites. In sample B4, one subordinated resolved peak at around 58.17 ppm was attributed to a minor four-coordinate tetrahedral Al core. The results obtained for FTIR, TGA, and NMR were in agreement with the chemical analyses shown above.

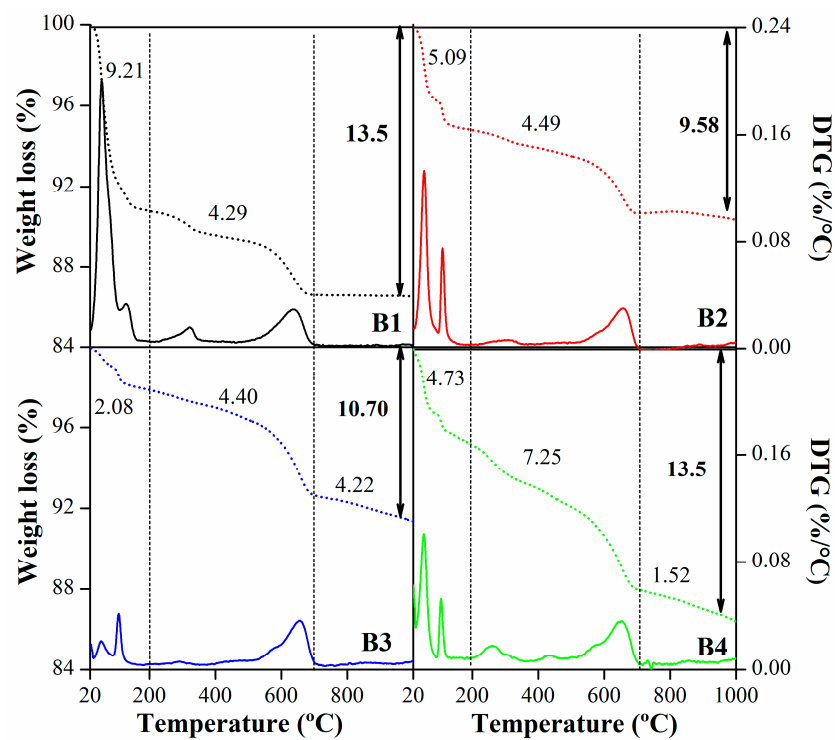


Figure 5. TGA (full lines) and DTG (dot lines) for the four bentonites and the percentage of weight loss in the different ranges.

3.1.2. Physical and Physicochemical Properties

Table 4 summarises the results of the cation exchange capacity determination, water content, swelling index, and colour parameters for four bentonites. The CEC values obtained are consistent with the high montmorillonite content and are similar to the values that were previously reported for materials from nearby sites [15,16,20]. Considering that three of the samples belong to the Allen Formation (AF) and the other to the Neuquén group (GN), only two, namely, B1 (GN) and B3 (FA), were chosen to determine the type of cations present. The results are shown in Figure 6 and indicate that B1 has a preponderance of divalent cations (Mg^{2+} and Ca^{2+}). In contrast, sample B3 is mostly monovalent (Na^+ and K^+), and the predominant cation is sodium. These results are in accordance with those obtained by XRD and enable the identification of samples B2, B3, and B4 as Na-bentonites and sample B1 as Mg-Ca-Na-bentonite.

Table 4. Physical and physicochemical properties of clay minerals.

	CEC ($cmol\ kg^{-1}$)	Swelling ($mL\ g^{-1}$)	Water Content (%)	Colour Parameters			Silt (%)	Clay (%)	Dv50 (μm)	Dv90 (μm)	D [3,4] (μm)
				L^*	a^*	b^*					
B1	99.56	<5.00	7.16	79.44	0.36	7.18	83.70	3.60	40.30	99.00	47.30
B2	92.83	6.75	7.43	88.95	0.55	3.96	86.10	2.70	43.60	92.50	47.90
B3	98.16	15.00	6.93	80.40	-0.39	11.1	97.10	3.20	35.00	78.50	39.90
B4	94.79	15.75	6.50	78.53	0.14	12.9	93.40	3.10	36.60	84.00	42.10

L^* , a^* , and b^* parameters were measured. L^* represents brightness (0 = black, and 100 = white), the a^* scale indicates the chromaticity axis ranging from green (-) to red (+), and the b^* axis ranges from blue (-) to yellow (+).

The values obtained for the swelling index suggested that two different types of behaviour could be considered and are associated with the deposit region. B1 is the bentonite with the least expansion capacity, which could be due to the presence of a divalent cation in the interlayer region keeping the clay sheets together with a greater force and requiring more energy for the layer expansion. The swelling values obtained for B3 and B4 are similar to those reported in previous research and are consistent with the fact

that sodium is the main cation in their interlayers [27]. In the case of B2, despite being a sodium bentonite, it has a low swelling percentage, which could suggest that this sample had a higher proportion of divalent cations in the interlayer than the other Na-bentonites. Further studies will be necessary to corroborate this. The values for water content were similar for all the samples and indicated that the water content is more weakly bound to the clay mineral surface. These values could be associated with the porosity of the samples, which must be mesoporosity for the montmorillonites.

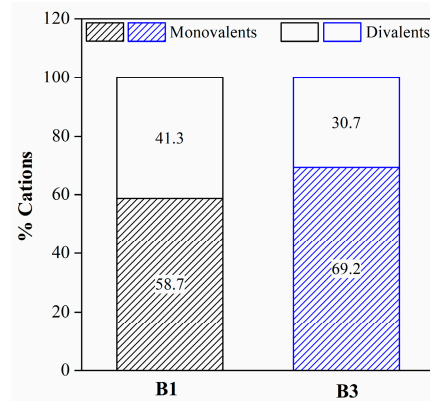


Figure 6. Percentage of divalent and monovalent cations in samples B1 (NG) and B3 (AF).

Figure 7 shows the cumulative volume and particle size distribution, and Table 4 summarises the main values obtained for four bentonites using gravimetric studies. The results showed that B1 had the highest percentage of clay and the lowest percentage of silt. The Na-bentonites that originated from the Lake Pellegrini deposit have similar compositions of silt and clay, and B2 had the lowest proportion of clay, which could be due its region of origin (Figure 7A). In all cases, the amount of clay present in each sample had a directly proportional relationship with quantity of smectite shown above (Table 1). The four samples have mostly unimodal particle size distributions with a particle size of less than 200 μm , according to the results previously shown (Figure 7B). Additionally, the values for Dv50 and Dv90 and the D [3,4] indicate that B1 and B2 are the minerals with the largest particle size. In contrast, B3 and B4 showed lower values, and this may be explained by the region from which each sample originated (Table 4).

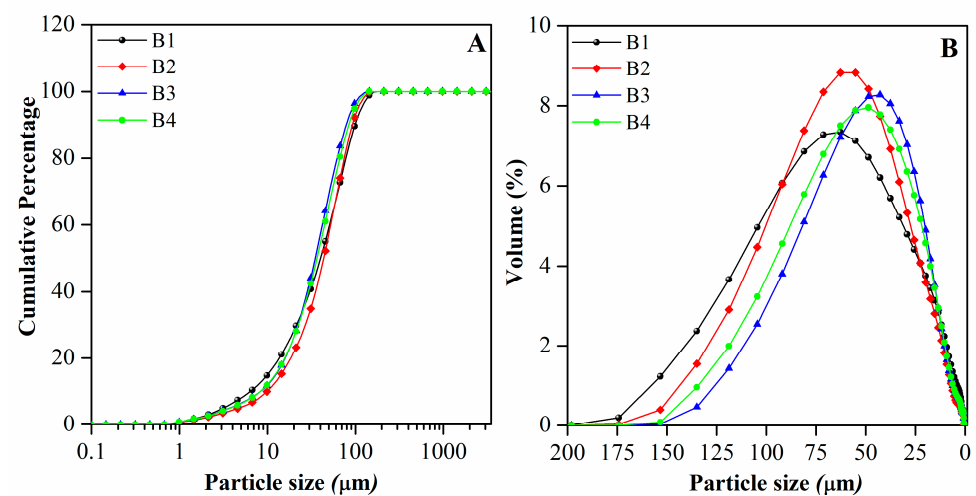


Figure 7. (A) Cumulative percentage. (B) Particle size distribution for bentonites.

The colour of the minerals was directly associated with their chemical and mineralogical composition. Colour is a relevant parameter when minerals are used in applications associated with health because colour is an important factor in their acceptability by people.

The colour of the bentonites are variable, ranging from blue-grey, olive, and brown to rarely white. White bentonites are very rare in occurrence and are more valuable in many applications that desire a white colour [47]. The colour parameters of the samples are shown in Table 4 where L^* , a^* , and b^* parameters were measured. L^* represents brightness (0 = black, and 100 = white), the a^* scale indicates the chromaticity axis ranging from green (−) to red (+), and the b^* axis ranges from blue (−) to yellow (+) [48]. High values of L^* indicate a greater capacity to reflect light, while low values represent a greater capacity to absorb electromagnetic radiation. The L values obtained for the samples indicate a scale of capacity to reflect increasing radiation in the order of $B4 < B1 < B3 \ll B2$. The first three samples are more similar to each other, while B2 differs markedly. With regard to parameter a^* , B3 presented chromaticity closer to green, while B2 tended more towards red. Regarding the chromaticity parameter b^* , all samples tended more towards yellow, with sample B3 having the highest value.

3.2. Anthocyanin Adsorption

Figure 8 shows the adsorption results when all the materials were probed as ACy adsorbents at pH 3, as mentioned above, and the pH was chosen taking into consideration the stability of the ACy solutions [1]. The results showed that the amount adsorbed by the samples was in the order of $B3 > B4 > B2 > B1$, suggesting that Na-bentonites have a higher ACy adsorption capacity than the Mg-Ca-Na-bentonite. This can be explained by considering that the adsorption mechanism reported for natural clays is cation exchange, and a monovalent cation, such as sodium, is more easily displaced than a divalent cation, such as calcium or magnesium. Thus, the flavylium cation present in the solution does not have sufficient strength to displace the divalent cations present in B1, decreasing its adsorption under these conditions.

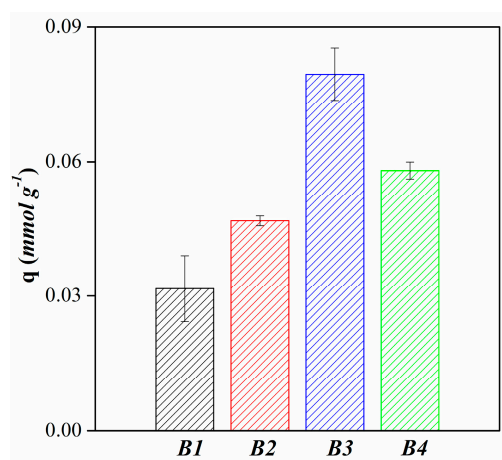


Figure 8. Adsorption of ACys on four bentonites.

Taking these results into account and to evaluate the pH required to carry out the kinetic and adsorption experiments, the sample B3 was chosen and the results of adsorption vs. pH are shown in Figure 9. This figure shows that the highest adsorption capacity was obtained at pH 3. As the pH values increased, the adsorption decreased significantly. These results may be explained by the fact that the clay has a net negative structural charge throughout the pH range and that the main ACy species in solution is the flavylium cation, which implies that the amount adsorbed will be greater at the lowest mean pH. This behaviour is associated with the adsorption mechanism of the cationic exchange of the flavylium cation by the cations in the natural material, which is well known. As the pH of the media increases because the proportion of uncharged ACy molecules (quinoidal base) increases, the adsorption is gradually reduced. Taking these results into account, the pH selected for the kinetic studies was pH 3.

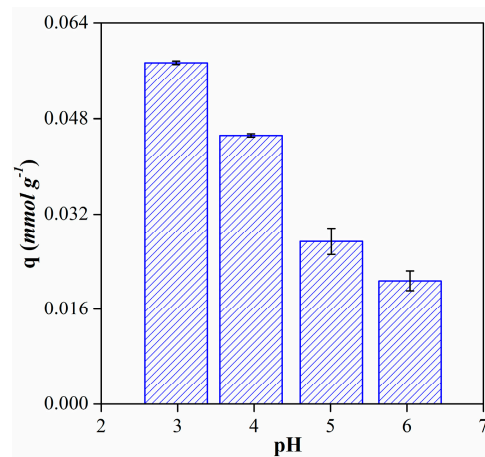


Figure 9. Adsorption of ACys on B3 vs. pH media.

Considering that the kinetics studies showed similar results for the sodic bentonites, Figure 10 shows the adsorption kinetics obtained for the B1 and B3 samples and their corresponding best fit. The results proved that the system quickly tends to equilibrium, with Na-bentonite reaching equilibrium after 1 h contact. Conversely, in the case of B1, the time necessary for the system to reach equilibrium was 4 h. Both results support the fact that the adsorption of ACys under these working conditions occurs by cation exchange because this type of mechanism has fast kinetics.

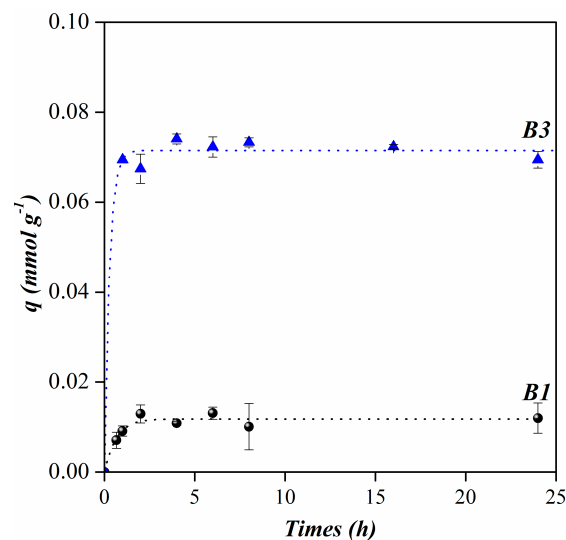


Figure 10. Kinetic adsorption data for ACys on B1 and B3 and their best adjustments.

The experimental data obtained were fitted to the PFO and PSO models, and Table 5 summarises the kinetic parameters calculated through nonlinear regression. As can be seen, the results exhibit a good fit for both models, but some slight differences can be observed. In the case of the B1 sample, the best fitting was obtained for the PFO model, suggesting that for this system, the adsorption process depends on the diffusion of ACy molecules from the bulk to the surface and their concentration [36]. For the B3 sample, the best fit was noted for the PSO model, which is based on the adsorption capacity of the solid, and the controlling stage of the adsorption process is the change generated in the system by either a chemical or electrostatic process. The latter would be the case for the adsorption of the flavylium cation through cation exchange.

Figure 11 shows the adsorption isotherms of ACys on all minerals at pH 3 and 20 °C. According to the classification by Giles et al. (1974) [49], the B1 isotherm can be classified as

Type S (sigmoidal). This finding suggests that at the beginning of the adsorption process, the ACy molecule has low affinity for the clay surface. However, once the adsorbate is retained in the solid, there could be new adsorption sites for other molecules. Samples B2 and B4 show Type L (Langmuir) isotherms, which suggests that there is a considerable affinity of the ACy species in solution towards the adsorbent, reaching a maximum adsorption value under the conditions studied. Finally, the isotherm obtained for B3 can be classified as Type H (high affinity), showing that at low ACy concentrations, a significant increase in adsorption occurs, proving that the affinity of the adsorbate for the adsorbent is considerably higher than the other samples [49–51]. Type L and Type H isotherms are associated with the adsorption of ionic solutes where there is no competition between the solute and the solvent for adsorption sites. These results support those previously proposed where the ACy species interacts electrostatically with the surface of the materials B2, B3, and B4 through a cationic exchange mechanism. In the case of sample B1, a higher ACy concentration is required to begin adsorption potentially because the one positive charge of the flavylum cation does not have sufficient strength to displace the divalent cations present in the interlayer of this material. Additionally, the latter is in agreement with the cooperative adsorption mechanism proposed for ACy adsorption on B1.

Table 5. Pseudo-first and pseudo-second order parameters calculated for ACy adsorption on B1 and B3 at pH 3 and 20 °C.

		B1	B3
Pseudo-first order	q_e (mmol g ⁻¹)	0.01	0.07
	k_1 (min ⁻¹)	0.03	0.06
	R^2	0.92	0.99
Pseudo-second order	q_e (mmol g ⁻¹)	0.01	0.07
	k_2 (g·(mmol min) ⁻¹)	3.86	3.35
	R^2	0.89	0.99

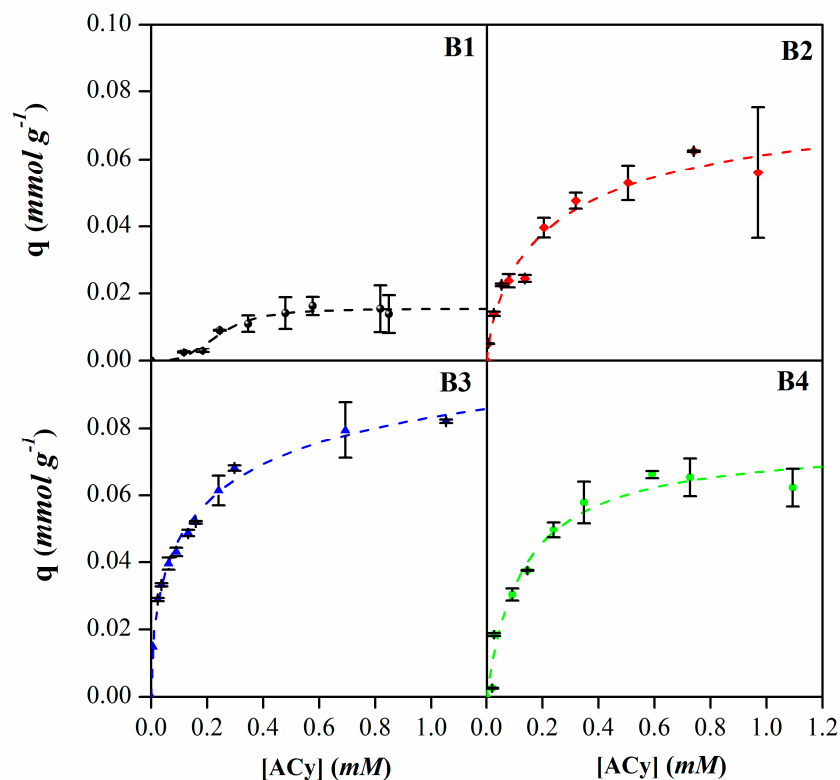


Figure 11. Experimental isotherms (symbols) and their best adjustments for the equilibrium adsorption data of ACy on four bentonites at pH 3 and 20 °C.

The experimental adsorption data were fitted to the Langmuir, Freundlich, and Sips models, and the corresponding fitting parameters are summarised in Table 6. Subsequently, Langmuir separation factors (R_L) were calculated for all systems, resulting in values of 0.41, 0.12, 0.05, and 0.10 for B1, B2, B3, and B4, respectively [38]. These values indicate a favorable adsorption process in all cases. Notably, the higher R_L value for B1 could be attributed to a more linear adsorption, potentially explained by the previously proposed cooperative adsorption mechanism.

Table 6. Freundlich, Langmuir, and Sips parameters for ACy adsorption on bentonites at pH 3 and 20 °C.

		B1	B2	B3	B4
Langmuir	q_m (mmol g ⁻¹)	0.03	0.07	0.08	0.07
	k (L mmol ⁻¹)	1.64	6.53	14.32	7.60
	R^2	0.87	0.96	0.95	0.97
	R_L	0.41	0.12	0.05	0.10
Freundlich	k_f (L g ⁻¹)	0.02	0.07	0.09	0.07
	n	1.62	2.61	3.53	2.82
	R^2	0.83	0.95	0.98	0.89
Sips	q_m (mmol g ⁻¹)	0.02	0.08	0.12	0.07
	b (L mmol ⁻¹) ^{1/n}	4.17	3.90	3.96	8.67
	n	0.29	1.32	1.88	0.84
	R^2	0.96	0.96	0.99	0.97

In all cases, the Sips model exhibited the best fit, suggesting that the adsorption systems exhibit heterogeneity. This could be attributed to ACy being adsorbed at sites with varying energy on the surface of the minerals or the presence of different ACy species in the solution. The ACy adsorption capacities followed the order of B1 < B4 < B2 and B3. This finding is consistent with the earlier results, where the amount of adsorbed ACy on Mg-Ca-Na-bentonite was considerably lower than in the B3 sample, owing to the higher concentration of divalent cations in the former. Among the Na-bentonites, B3 had a comparable CEC values to the others, suggesting that the higher adsorption obtained may be due to other samples having higher contributions of divalent cations, such as calcium or magnesium, in their structure than B3, consequently reducing their adsorption capacities. The latter finding is made according to observations in the chemical analyses of bentonites. Additionally, the values obtained for parameter n , associated with system heterogeneity, indicated that B1 and B4 samples have values less than 1, indicating more homogeneous systems, while B2 and B3 exhibit higher heterogeneity. These results correlate with the adsorption capacities obtained for each material, suggesting that higher heterogeneity enhances ACy adsorption onto the samples under the studied conditions.

In order to investigate whether the adsorption of ACy on the bentonites was by cationic exchange in all cases, the adsorption complexes of ACy on the four samples were analysed. For this, adsorption was carried out under the same conditions as previously described. The supernatant was separated, and the solids were dried at room temperature. FTIR and XRD analyses were obtained for each of the samples. Figure 12 shows the diffractograms of the ACy–bentonite complexes obtained. For B2, B3, and B4, an increase of 1.2 to 1.4 nm in the basal spacing d_{001} was observed. It is well known that sodium montmorillonites have a hydration layer of the sodium cation and are identified by the presence of a d_{001} that appears in the vicinity of 1.26 nm, a value that includes the thickness of a TOT sheet (0.96 nm) plus the interlaminal space that will vary depending on the interlayer cation and its hydration [52]. Because the laminar structure of the mineral is not modified during the adsorption process, the increase in the basal space demonstrates that the anthocyanin molecules were adsorbed in the interlaminal space of the sodium bentonites, which concurs with similar results reported for other ACy–clay systems [9,11,12,53]. Likewise, the width of the peaks obtained suggests a higher disorder in the interlayer of the complexes obtained

than the natural material, which could be explained by the contribution made by different interlaminal spaces generated by different orientations of the ACy molecule adsorbed in the interlayer of the material. In the case of B1, it was observed that the basal spacing decreased from 1.46 nm, which is characteristic of bentonites with a predominance of divalent cations, to a value of 1.22 nm, which could indicate that the ACys were adsorbing in a position such that the smallest possible space is occupied. Alternatively, ACys are adsorbed outside the interlayer through other types of interactions. The latter could be because the ACy molecule adsorbs on the non-charged surface sites on B1, such as the siloxane surface, and through hydrophobic interactions, which would explain the cooperative adsorption mechanism proposed.

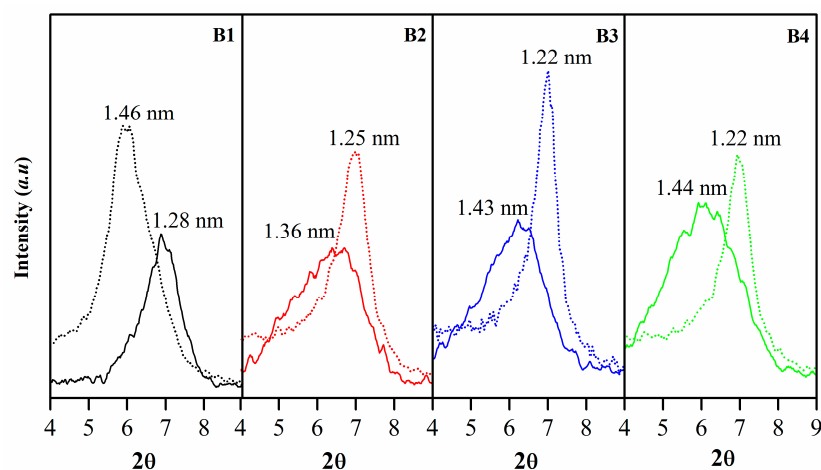


Figure 12. ACy–bentonites complex diffractograms and raw materials.

A possible explanation for the results obtained for the XRD analysis of the ACy–bentonite complexes derived from analysing the structure and dimensions of the ACy molecule is shown in Figure 13. This figure shows that there is a fraction of the molecule composed of aromatic rings, which is flat (flavylium cation), while the glucoside substituents, due to their characteristic boat-shaped structure, generate a region of greater spatial distribution. Based on this finding, it could be inferred that, in the case of the sodium bentonites, the molecule gets into the interlaminal space in the conformation represented as B, where the aromatic rings of the flavylium cation in the ACy molecule remain parallel to the internal surface, resulting in a basal spacing that is the sum of the thickness of the ACy molecule (0.46 nm) and the TOT sheet (0.96 nm). The latter is in agreement with previous reports that suggest that molecules with aromatic rings can orient themselves in the interlayer of the clay mineral and interact through hydrophobic interactions with the siloxane surface of the tetrahedral sheet and with the previously proposed cation exchange mechanism [11]. However, it can be seen that the maximum quantity of adsorbed ACys is low compared to the CEC of each of the bentonites. A possible explanation for this fact would be to consider the molecular size of the ACy. In addition, once the molecule is adsorbed, the neighbouring adsorption sites are blocked, preventing the entry of new ACy molecules into the structure. In the case of B1, and as mentioned above, the molecule may be adsorbed mostly on the external surface of siloxane. After that, it becomes an adsorption site for other molecules, favouring cooperative adsorption.

The FTIR spectra obtained for the ACy–bentonite complex show the same signals and are illustrated in Figure 14. The absorption peaks at 3620, 3430, and 1030 cm^{-1} are characteristic of montmorillonites and correspond to the stretching of the O–H bonds located between the tetrahedral and octahedral sheets of the mineral, the vibration of the O–H bonds of the water molecules, and the stretching of Si–O, respectively [42,54]. These results showed that the structure of the mineral did not suffer modifications following the adsorption of ACys on the surface (see Figure 14A). Conversely, in Figure 14B, the

absorption observed at 2928 cm^{-1} is associated with the scissor bending of the $-\text{CH}_2-$ groups in the cyclohexanes, while the bands between 1736 cm^{-1} and 1697 cm^{-1} refer to the out-of-plane bending of the C–H bonds. These bands may appear superimposed on the broadband that appears around 1600 cm^{-1} related to the hydration water of the clay mineral. Finally, the set of bands between $1585\text{--}1543\text{ cm}^{-1}$ and 1508 cm^{-1} are associated with the conjugated diene groups, and this may be due to the interaction of this fraction of the molecule with the natural material [7,55].

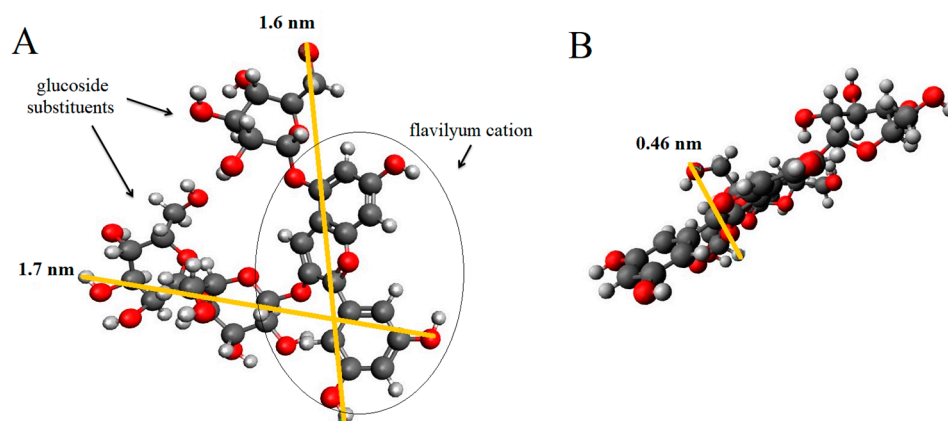


Figure 13. Spatial representation from different views (A) and (B) and dimensions (yellow lines) of the molecule cyanidin-3-diglucoside-5-glucoside molecule.

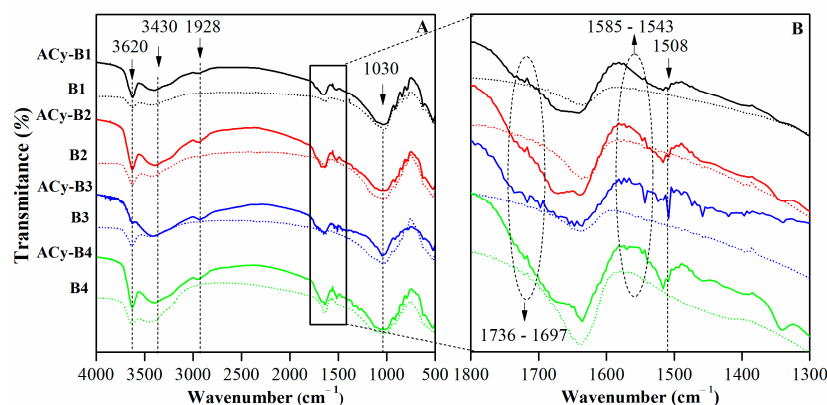


Figure 14. (A) FTIR spectra of the ACy-bentonite complex. (B) Enlargement in the range of 1800 to 1300 cm^{-1} .

The last adsorption probe was to evaluate the material that showed the highest adsorption capacity at a pH value higher than 3, and pH 4.5 was chosen due to the instability of the Acy molecule. Figure 15 shows the adsorption isotherms of ACys on B3 at pH 3 and 4.5. The isotherm obtained at pH 3 was previously analysed and classified as Type L according to the classification proposed by Giles et al. [49] where the adsorption is the result of the cation exchange of the flavilyum cation present in the solution. The isotherm obtained at pH 4.5 is a sigmoidal type isotherm (Type S), indicating cooperative adsorption, similar to that observed for B1 at pH 3. This could be explained by changes in the pH of the medium. Here, as the pH increases, the concentration of the flavilyum cation decreases, and the neutral species (carbinol pseudobase) appear [56,57]. In this case, the adsorption generated by cation exchange will be considerably lower, and the species present could be adsorbing through other types of mechanisms, such as van der Waals type interactions or hydrogen bonding, among others, which is consistent with the cooperative adsorption previously proposed [11,58].

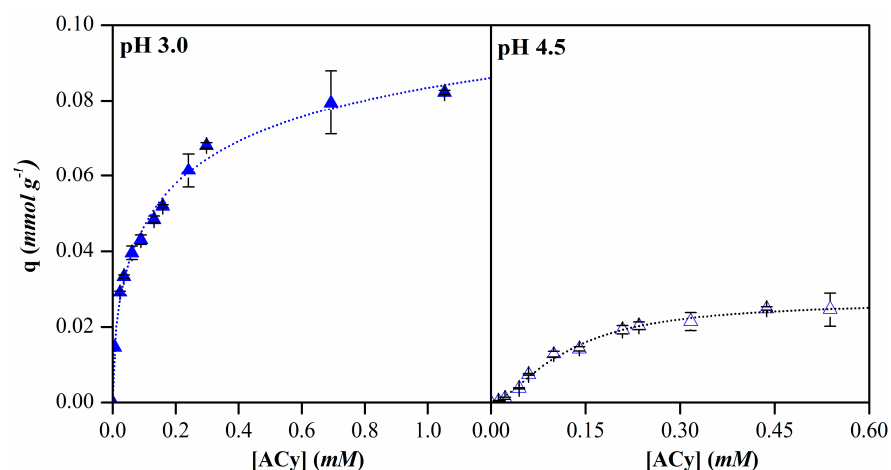


Figure 15. Experimental isotherms (symbols) and their best equations adjustments for the equilibrium adsorption data of ACys on B3 at pH 3 and 4.5.

The experimental data were fitted to the Langmuir, Freundlich, and Sips models, with the best fits obtained for the Sips model (see Table 7). The obtained R_L values were 0.05 and 0.27 for pH 3 and 4.5, respectively, indicating a favorable adsorption process. Similar to previous observations, the highest adsorption capacity and the n parameter value were obtained at pH 3, demonstrating that increased heterogeneity indeed leads to a higher ACy adsorption capacity. However, in this case, the high heterogeneity could be associated with different ACy species present in solution at pH 3 that are not present at pH 4.5 and could interact with the surface at different available sites [56,57]. The results presented include those obtained and shown previously.

Table 7. Freundlich, Langmuir, and Sips parameters for ACy adsorption on B3 at pH 3 and 4.5.

		pH 3.0	pH 4.5
Langmuir	q_m (mmol g ⁻¹)	0.08	0.04
	k (L mmol ⁻¹)	14.32	4.51
	R^2	0.95	0.98
Freundlich	k_f (L g ⁻¹)	0.09	0.04
	n	3.53	1.76
	R^2	0.98	0.93
Sips	q_m (mmol g ⁻¹)	0.12	0.03
	b (L mmol ⁻¹) ^{1/n}	3.96	8.57
	n	1.88	0.61
	R^2	0.99	0.99

The results reported by various authors in recent years for the ACys from red cabbage adsorption on different adsorbents are summarised in Table 8 and compared with the results obtained at pH 3 in this study. As can be seen, there are many solids with the ability to adsorb ACys from red cabbage, with a notable scarcity of reports on natural clays. The adsorption of ACys onto diverse materials is primarily contingent upon the inherent characteristics of the adsorbent, encompassing its chemical composition, physical and textural properties, and operational conditions (pH, temperature, ionic strength, etc.). Notably, the results obtained for samples B2, B3, and B4 significantly surpass the majority of reported materials. Across all instances, the natural bentonites examined in this study emerge as exceptional adsorbents for ACys in aqueous environments.

Table 8. ACy adsorption capacities for different materials.

Adsorbent	$q_{m,ACy}$ (mmol g ⁻¹)	Reference
Porous clay heterostructure synthesised from the bentonite sample	0.02	[59]
Sepiolite	0.02	
Chitosan film at 298 K	0.33	[60]
X-5 Microporous resin	0.03	[61]
Clay Tonsil Terrana 580 FF	0.02	[62]
Clay HDPE nanocomposite	0.02	
B1	0.02	This work
B2	0.08	
B3	0.12	
B4	0.07	

4. Conclusions

In the present work, four bentonites from the northern Patagonian region were thoroughly characterised and evaluated as possible adsorbents of a natural dye present in red cabbage (ACy).

The results showed that three of these samples, belonging to the Allen Formation, can be considered Na-bentonites due to their composition and physicochemical properties. The fourth belongs to the Neuquén Group and contains an important proportion of divalent cations in its structure, in particular magnesium and calcium, which allows it to be characterised as Mg-Ca-Na-bentonite.

The ACy adsorption studies conducted on the four materials demonstrated that Na-bentonites exhibit superior adsorption of ACys from red cabbage compared to Mg-Ca-Na-bentonite under the investigated conditions. This latter evidence indicates that the charge of the cation present in the interlayer and the species of ACy present in the solution considerably influence the quantity of ACys that the material can retain. The B3 sample showed the highest ACy adsorption capacity among the Na-bentonites probably due to its elevated CEC and smectite proportion.

Furthermore, all Na-bentonites exhibit higher ACy adsorption capacities compared to values reported for other materials and provide strong evidence that the materials examined in this study can serve as exceptional adsorbents for ACy extracted from red cabbage under the specified conditions.

The analysis of ACy–bentonite adsorption complexes confirmed the presence of ACys in the interlayer of Na-bentonites, indicating that ACys were adsorbed through a cationic exchange mechanism. In contrast, ACys on Mg-Ca-Na-bentonite were exclusively adsorbed through other types of interactions. These results are significant given that there are previous reports regarding the adsorption of ACys extracted from other natural sources that suggest that once ACy molecules are adsorbed in the interlayer of smectite, their stability is considerably increased compared to that observed in aqueous solution. The latter is an extremely interesting result given that it represents a potentially new field of application for regional materials that has not been evaluated to date.

Author Contributions: Conceptualisation: V.R.-A. and M.E.R.-J.; methodology: V.R.-A. and A.M.; formal analysis: V.R.-A., M.B.G. and M.E.R.-J.; investigation: V.R.-A., M.B.G., M.E.R.-J., P.M.N. and M.P.; resource: M.E.R.-J., P.M.N. and M.P.; data curation: V.R.-A., M.B.G. and A.M.; writing—original draft preparation: V.R.-A., M.P. and M.E.R.-J.; writing—review and editing: V.R.-A., M.P. and M.E.R.-J.; project administration: M.E.R.-J. and M.P.; funding acquisition: M.P. and M.E.R.-J. All authors have read and agreed to the published version of the manuscript.

Funding: This research was funded by the National University of Comahue under the Project I04-249, titled “Natural and Modified Clay Minerals for Applications in Health and Environment”, within the Faculty of Engineering.

Data Availability Statement: Data are contained within the article.

Acknowledgments: The authors gratefully acknowledge PROBIEN-CONICET-UNCo and Autonomous University of Madrid for providing technological support.

Conflicts of Interest: The authors declare no conflicts of interest.

References

1. Pourjavaher, S.; Almasi, H.; Meshkini, S.; Pirsá, S.; Parandi, E. Development of a colorimetric pH indicator based on bacterial cellulose nanofibers and red cabbage (*Brassica oleraceae*) extract. *Carbohydr. Polym.* **2017**, *156*, 193–201. [[CrossRef](#)]
2. Ghareaghajlou, N.; Hallaj-Nezhadi, S.; Ghasempour, Z. Red cabbage anthocyanins: Stability, extraction, biological activities and applications in food systems. *Food Chem.* **2021**, *365*, 130482. [[CrossRef](#)]
3. McDougall, G.J.; Fyffe, S.; Dobson, P.; Stewart, D. Anthocyanins from red cabbage—stability to simulated gastrointestinal digestion. *Phytochemistry* **2007**, *68*, 1285–1294. [[CrossRef](#)]
4. Saluk, J.; Bijak, M.; Kołodziejczyk-Czepas, J.; Posmyk, M.M.; Janas, K.M.; Wachowicz, B. Anthocyanins from red cabbage extract—evidence of protective effects on blood platelets. *Cent. Eur. J. Biol.* **2012**, *7*, 655–663. [[CrossRef](#)]
5. Benvenuti, S.; Bortolotti, E.; Maggini, R. Antioxidant power, anthocyanin content and organoleptic performance of edible flowers. *Sci. Hortic.* **2016**, *199*, 170–177. [[CrossRef](#)]
6. Wiczowski, W.; Szawara-Nowak, D.; Topolska, J. Red cabbage anthocyanins: Profile, isolation, identification, and antioxidant activity. *Food Res. Int.* **2013**, *51*, 303–309. [[CrossRef](#)]
7. Li, S.E.; Mu, B.; Ding, J.; Zhang, H.; Wang, X.W.; Wang, A.Q. Fabrication of anthocyanin/ montmorillonite hybrid pigments to enhance their environmental stability and application in allochromic composite films. *Clays Clay Min.* **2021**, *69*, 142–151. [[CrossRef](#)]
8. Amogne, N.Y.; Ayele, D.W.; Tsigie, Y.A. Recent advances in anthocyanin dyes extracted from plants for dye sensitized solar cell. *Mater. Renew. Sustain. Energy* **2020**, *9*, 23. [[CrossRef](#)]
9. Kohno, Y.; Yasushi, K.; Shibata, M.; Fukuhara, C.; Maeda, Y.; Tomita, Y.; Kobayashi, K. Enhanced stability of natural anthocyanin incorporated in Fe-containing mesoporous silica. *Microporous Mesoporous Mater.* **2015**, *203*, 232–237. [[CrossRef](#)]
10. Kohno, Y.; Haga, E.; Yoda, K.; Shibata, M.; Fukuhara, C.; Tomita, Y.; Maeda, Y.; Kobayashi, K. Adsorption behavior of natural anthocyanin dye on mesoporous silica. *J. Phys. Chem. Solids* **2014**, *75*, 48–51. [[CrossRef](#)]
11. Kohno, Y.; Kinoshita, R.; Ikoma, S.; Yoda, K.; Shibata, M.; Matsushima, R.; Tomita, Y.; Maeda, Y.; Kobayashi, K. Stabilization of natural anthocyanin by intercalation into montmorillonite. *Appl. Clay Sci.* **2009**, *42*, 519–523. [[CrossRef](#)]
12. Kohno, Y.; Hoshino, R.; Matsushima, R.; Tomita, Y.; Kobayashi, K. Stabilization of Flavylum Dyes by Incorporation in the Clay Interlayer. *J. Jpn. Soc. Colour. Mater.* **2007**, *80*, 6–12. [[CrossRef](#)]
13. Silva, G.T.M.; Silva, C.P.; Gehlen, M.H.; Oake, J.; Bohne, C.; Quina, F.H. Organic/inorganic hybrid pigments from flavylum cations and palygorskite. *Appl. Clay Sci.* **2018**, *162*, 478–486. [[CrossRef](#)]
14. Brown, T.J.; Idoine, N.E.; Raycraft, E.R.; Shaw, R.A.; Hobbs, S.F.; Everett, P.; Deady, E.A.; Bide, T. World Mineral Production 2012–2016. In *British Geological Survey; World Mineral Statistics*: Nottingham, UK, 2018.
15. Musso, T.B.; Roehl, K.E.; Pettinari, G.; Vallés, J.M. Assessment of smectite-rich claystones from Northpatagonia for their use as liner materials in landfills. *Appl. Clay Sci.* **2010**, *48*, 438–445. [[CrossRef](#)]
16. Lombardi, B.; Baschini, M.; Torres Sánchez, R.M. Bentonite deposits of Northern Patagonia. *Appl. Clay Sci.* **2003**, *22*, 309–312. [[CrossRef](#)]
17. Parolo, M.E.; Avena, M.J.; Pettinari, G.R.; Baschini, M.T. Influence of Ca²⁺ on tetracycline adsorption on montmorillonite. *J. Colloid. Interface Sci.* **2012**, *368*, 420–426. [[CrossRef](#)] [[PubMed](#)]
18. Parolo, M.E.; Savini, M.C.; Vallés, J.M.; Baschini, M.T.; Avena, M.J. Tetracycline adsorption on montmorillonite: pH and ionic strength effects. *Appl. Clay Sci.* **2008**, *40*, 179–186. [[CrossRef](#)]
19. Parolo, M.E.; Avena, M.J.; Pettinari, G.; Zajonkovsky, I.; Valles, J.M.; Baschini, M.T. Antimicrobial properties of tetracycline and minocycline-montmorillonites. *Appl. Clay Sci.* **2010**, *49*, 194–199. [[CrossRef](#)]
20. Roca Jalil, M.E.; Baschini, M.; Sapag, K. Influence of pH and antibiotic solubility on the removal of ciprofloxacin from aqueous media using montmorillonite. *Appl. Clay Sci.* **2015**, *114*, 69–76. [[CrossRef](#)]
21. Roca Jalil, M.E.; Vieira, R.S.; Azevedo, D.; Baschini, M.; Sapag, K. Improvement in the adsorption of thiabendazole by using aluminum pillared clays. *Appl. Clay Sci.* **2013**, *71*, 55–63. [[CrossRef](#)]
22. Lombardi, B.; Baschini, M.; Torres Sánchez, R.M. Optimization of parameters and adsorption mechanism of thiabendazole fungicide by a montmorillonite of North Patagonia, Argentina. *Appl. Clay Sci.* **2003**, *24*, 43–50. [[CrossRef](#)]
23. Carretero, M.I.; Pozo, M. Clay and non-clay minerals in the pharmaceutical industry. Part I. Excipients and medical applications. *Appl. Clay Sci.* **2009**, *46*, 73–80. [[CrossRef](#)]
24. Carretero, M.I.; Pozo, M. Clay and non-clay minerals in the pharmaceutical and cosmetic industries Part II. Active ingredients. *Appl. Clay Sci.* **2010**, *47*, 171–181. [[CrossRef](#)]

25. Moraes, J.D.D.; Bertolino, S.R.A.; Cuffini, S.L.; Ducart, D.F.; Bretzke, P.E.; Leonardi, G.R. Clay minerals: Properties and applications to dermocosmetic products and perspectives of natural raw materials for therapeutic purposes—A review. *Int. J. Pharm.* **2017**, *534*, 213–219. [[CrossRef](#)] [[PubMed](#)]
26. Roca Jalil, M.E.; Sanchez, M.; Pozo, M.; Soria, C.; Vela, L.; Gurnik, N.; Baschini, M. Assessment of natural and enhanced peloids from the Copahue thermal system (Argentina): Effects of the drying procedure on lidocaine adsorption. *Appl. Clay Sci.* **2020**, *196*, 105751. [[CrossRef](#)]
27. Iborra Viseras, C.; Cultrone, G.; Cerezo, P.; Aguzzi, C.; Baschini, M.T.; Vallés, J.; López-Galindo, A. Characterisation of northern Patagonian bentonites for pharmaceutical uses. *Appl. Clay Sci.* **2006**, *31*, 272–281. [[CrossRef](#)]
28. Caminos, R.; Chernicoff, C.J.; Fauqué, L.; Franchi, M. *Hoja Geológica 4166-I Valcheta*; Provincia de Río Negro; Boletín 310-73; Instituto de Geología y Recursos Minerales: Buenos Aires, Argentina, 2001.
29. Johannis, P.; Dalponte, M.; Juárez, P.; Giacosa, R. Recursos minerales industriales, rocas de aplicación y gemas de la provincia de Río Negro. In *Serie Contribuciones Técnicas Recursos Minerales N° 49*; Servicio Geológico Minero Argentino: Buenos Aires, Argentina, 2022; Volume 49, pp. 1–97. Available online: <https://repositorio.segemar.gov.ar/handle/308849217/4249> (accessed on 29 December 2023).
30. Giusti, M.; Wroldstad, R. Characterization and Measurement of Anthocyanins by UV-Visible Spectroscopy. In *Current Protocols in Food Analytical Chemistry*; Servicio Geológico Minero Argentino: Buenos Aires, Argentina, 2001; pp. F1–F2.
31. Schultz, L.G. Quantitative Interpretation of Mineralogical Composition from X-ray and Chemical Data for the Pierre Shale. In *Geological Survey Professional Paper*; United States Government Printing Office: Washington, DC, USA, 1964.
32. Moore, D.M.; Reynolds, R.C. *X-ray Diffraction and the Identification and Analysis of Clay Minerals*, 2nd ed.; Oxford University Press: Oxford, UK, 1997; p. 378.
33. Massiot, D.; Bessada, C.; Coutures, J.P.; Taulelle, F. A quantitative study of ²⁷Al MAS NMR in crystalline YAG. *J. Magn. Reson.* (1969) **1990**, *2*, 231–242. [[CrossRef](#)]
34. Meier, L.P.; Kahr, G. Determination of the Cation Exchange Capacity (CEC) of Clay Minerals Using the Complexes of Copper (II) Ion with Triethylenetetramine and Tetraethylenepentamine. *Clays Clay Miner.* **1999**, *47*, 386–388. [[CrossRef](#)]
35. Mohd, P.; Khan, A.; Farooqui, M. Analytical Applications of Plant Extract as Natural pH Indicator: A Review. *J. Adv. Sci. Res.* **2011**, *2*, 20–27.
36. Vareda, J.P. On validity, physical meaning, mechanism insights and regression of adsorption kinetic models. *J. Mol. Liq.* **2023**, *376*, 121416. [[CrossRef](#)]
37. Wang, J.; Guo, X. Adsorption isotherm models: Classification, physical meaning, application and solving method. *Chemosphere* **2020**, *258*, 127279. [[CrossRef](#)] [[PubMed](#)]
38. Al-Ghouti, M.A.; Da'ana, D.A. Guidelines for the use and interpretation of adsorption isotherm models. A review. *J. Hazard. Mater.* **2020**, *393*, 122383. [[CrossRef](#)]
39. Greene-Kelly, R. The identification of montmorillonoids in clays. *J. Soil Sci.* **1953**, *4*, 232–237. [[CrossRef](#)]
40. Tabak, A.; Afsin, B.; Aygun, S.F.; Koksal, E. Structural characteristics of organo-modified bentonites of different origin. *J. Therm. Anal. Calorim.* **2007**, *87*, 377–382. [[CrossRef](#)]
41. Komadel, P.; Madejová, J. Chapter 7.1 Acid Activation of Clay Minerals. *Dev. Clay Sci.* **2006**, *1*, 263–287. [[CrossRef](#)]
42. Madejová, J. FTIR techniques in clay mineral studies. *Vib. Spectrosc.* **2003**, *31*, 1–10. [[CrossRef](#)]
43. Guggenheim, S.; Koster van Groos, A.F. Baseline studies of the clay minerals society source clays: Thermal analysis. *Clays Clay Miner.* **2001**, *49*, 433–443. [[CrossRef](#)]
44. Sorieul, S.; Allard, T.; Wang, L.; Grambin-Lapeyre, C.; Lian, J.; Calas, G.; Ewing, R. Radiation-stability of smectite. *Environ. Sci. Technol.* **2008**, *42*, 8407–8411. [[CrossRef](#)]
45. Önal, M.; Sarıkaya, Y. Thermal behavior of a bentonite. *J. Therm. Anal. Calorim.* **2007**, *90*, 167–172. [[CrossRef](#)]
46. Woessner, D.E. Characterization of clay minerals by ²⁷Al nuclear magnetic resonance spectroscopy. *Am. Mineral.* **1989**, *74*, 203–215.
47. Murray, H.H. Chapter 2: Structure and Composition of the Clay Minerals and their Physical and Chemical Properties. *Dev. Clay Sci.* **2006**, *2*, 7–31. [[CrossRef](#)]
48. Sette, P.; Fernandez, A.; Soria, J.; Rodriguez, R.; Salvatori, D.; Mazza, G. Integral valorization of fruit waste from wine and cider industries. *J. Clean. Prod.* **2020**, *242*, 118486. [[CrossRef](#)]
49. Giles, C.H.; Smith, D. A General Treatment and Classification of the Solute Adsorption Isotherm. *J. Colloid Interface Sci.* **1974**, *47*, 755–765. [[CrossRef](#)]
50. Limousin, G.; Gaudet, J.P.; Charlet, L.; Szenknect, S.; Barthès, V.; Krimissa, M. Sorption isotherms: A review on physical bases, modeling and measurement. *Appl. Geochem.* **2007**, *22*, 249–275. [[CrossRef](#)]
51. Saadi, R.; Saadi, Z.; Fazaali, R.; Fard, N.E. Monolayer and multilayer adsorption isotherm models for sorption from aqueous media. *Korean J. Chem. Eng.* **2015**, *32*, 787–799. [[CrossRef](#)]
52. Brigatti, M.F.; Galán, E.; Theng, B.K.G. Structure and Mineralogy of Clay Minerals. *Dev. Clay Sci.* **2013**, *5*, 21–81. [[CrossRef](#)]
53. Cunha, R.; Trigueiro, P.; Orta-Cuevas, M.; Medina-Carrasco, S.; Duarte, T.; Honório, L.; Damacena, D.; Fonseca, M.G.; da Silva-Filho, E.; Osajima, J. The Stability of Anthocyanins and Their Derivatives through Clay Minerals: Revising the Current Literature. *Minerals* **2023**, *13*, 268. [[CrossRef](#)]

54. Elkhalfah, A.; Murugesan, T.; Azmi-Bustam, M. Characterization of different cationic forms of montmorillonite by FTIR, XRD and TGA techniques. In Proceedings of the 2011 National Postgraduate Conference, Perak, Malaysia, 19–20 September 2011; pp. 1–6.
55. Silverstein, R.M.; Bassler, G.C. Spectrometric identification of organic compounds. *J. Chem. Educ.* **1962**, *39*, 546. [[CrossRef](#)]
56. Fenger, J.A.; Moloney, M.; Robbins, R.J.; Collins, T.M.; Dangles, O. The influence of acylation, metal binding and natural antioxidants on the thermal stability of red cabbage anthocyanins in neutral solution. *Food Funct.* **2019**, *10*, 6740–6751. [[CrossRef](#)]
57. Chigurupati, N.; Saiki, L.; Gayser, C.; Dash, A.K. Evaluation of red cabbage dye as a potential natural color for pharmaceutical use. *Int. J. Pharm.* **2002**, *241*, 293–299. [[CrossRef](#)]
58. Lima, E.; Martínez-Ortiz, M.J.; Fregoso, E.; Méndez-Vivar, J. Capturing natural chromophores on natural and synthetic aluminosilicates. *Stud. Surf. Sci. Catal.* **2007**, *170*, 2110–2115. [[CrossRef](#)]
59. Tavares Guimarães, D.; Ramos Mendes, L.M.; De Sousa Sabino, L.B.; De Brito, E.S.; Vilarrasa-García, E.; Rodríguez-Castellón, E.; Cecilia, J.A.; Da Silva, I.J., Jr. Partial Purification of Anthocyanins (*Brassica oleracea* var. Rubra) from Purple Cabbage Using Natural and Modified Clays as Adsorbent. *Adsorpt. Sci. Technol.* **2023**, *2023*, 2724122. [[CrossRef](#)]
60. Carvalho, V.L.; Gonçalves, J.O.; Silva, A.; Cadaval, T.R.; Pinto, L.A.; Lopes, T.J. Separation of anthocyanins extracted from red cabbage by adsorption onto chitosan films. *Int. J. Biol. Macromol.* **2019**, *131*, 905–911. [[CrossRef](#)] [[PubMed](#)]
61. Zhang, P.; Wang, L.; Fang, S. Modeling of the Adsorption/Desorption Characteristics and Properties of Anthocyanins from Extruded Red Cabbage Juice by Macroporous Adsorbent Resin. *Int. J. Food Eng.* **2019**, *15*, 20180239. [[CrossRef](#)]
62. Lopes, T.J.; Gonçalves, O.H.; Quadri, M.G.N.; Machado, R.A.F.; Quadri, M.B. Adsorption of anthocyanins using clay-polyethylene nanocomposite particles. *Appl. Clay Sci.* **2014**, *87*, 298–302. [[CrossRef](#)]

Disclaimer/Publisher's Note: The statements, opinions and data contained in all publications are solely those of the individual author(s) and contributor(s) and not of MDPI and/or the editor(s). MDPI and/or the editor(s) disclaim responsibility for any injury to people or property resulting from any ideas, methods, instructions or products referred to in the content.